



Droplets Generation Using Soluble Polymeric and Surfactant Additives in a Micro-Flow System: An Experimental Approach

Nur Farra Ilyana Binti Yosman^a, Wafaa K. Mahmood^b , Hayder A. Abdulbari^{a*}

^a Center of Excellence for Advanced Research in Fluid Flow, University Malaysia Pahang, 26300

^b Production Engineering and Metallurgy Dept., University of Technology-Iraq, Alsina'a street, 10066 Baghdad, Iraq.

*Corresponding author Email: abhayder@ump.edu.my

HIGHLIGHTS

- The effect of polymer on the flow behavior and droplet generation efficiency in a micro-flow system was investigated.
- The effect of the presence of Surfactant molecules on the droplet generation rate and droplets size, and flow behavior in a microfluidic chip was evaluated
- The jetting regions phenomena in a micro-flow system were investigated.

ARTICLE INFO

Handling editor: Mustafa H. Al-Furaiji

Keywords:

Microfluidics
Microdroplet generation
Polymeric Additives
Surfactants
Jetting Effect

ABSTRACT

In the present work, polymer and surfactant solutions (Xanthan Gum-Cetyltrimethylammonium bromide) were formulated and tested in a micro-flow system (microchannel) carrying octanoic acid as the hydrocarbon phase to determine the droplets formation capabilities of the two different additives. The purpose is to compare the droplet-generated size, shape, and distance between the droplets forming from the individual additives solutions. The jetting phenomenon that happens during droplet generation was also investigated. The solution of the polymer (XG) and surfactant (CTAB) was prepared in 5 different concentrations (50, 100, 150, 200, and 250) ppm and (500, 1000, 1500, 2000, and 2500) ppm, respectively. The continuous and dispersed phases' flow was controlled by controlling the inlet pressure of both phases. Direct-writing lithography was used to fabricate the microchannels using polydimethylsiloxane polymer. The microfluidic chip was connected to an open-loop fluid circulation system, and the produced by polymer and surfactant solutions droplets size was recorded using a high-resolution microscope. The droplet generated using the XG solution was larger, and the distance between droplets was shorter as concentration increased. In contrast, the CTAB solutions showed smaller droplets, and the distance between droplets increased as the concentration increased. The possibility of coalescence of the droplet was also higher as the distance between droplets was shorter. In terms of jetting regime, as the pressure ratio increases, the jet breakup length increases before forming the droplet until, at some limit, the dispersed phase was failed to generate droplets.

1. Introduction

Microfluidic technology's rapid advancements provided a great foundation for creating cutting-edge technologies and devices that may be employed in various applications, including biosensors, pharmaceuticals, diagnostic, and reaction engineering. Reaction and reactor optimization is an important subject where microfluidics technology has been effectively employed. Many researchers benefit from miniaturizing current reaction techniques to understand better the reaction mechanisms that drive the process and to analyze multiple known reaction methods.

Droplet-based microreactors attracted attention due to their high academic and commercial impact. For the past several years, advancements in science and technology have exhibited a breakthrough approach in introducing and utilizing microreactors technology in academics and enterprises. Micro-sized reactors have been used in the chemical, pharmaceutical, biotechnology, and even environmental diagnostic industries [1]. The innovative idea has grown fast owing to its superior efficiency to traditional macro-scale reactors [2,3,4,5]. The miniature devices provide high-throughput methods in chemical synthesis with higher yield and selectivity, improved sample consistency at lower reaction volume [6], and lower energy consumption [3,5,7]. Microreactors also demonstrated high mass and heat transfer rates and the ability to precisely control the fluids in terms of contact time, shape, and size of the fluids interface. This technology can lower the environmental impact while boosting process safety by reducing the number of reagents and solvents used [4]. The microreactors' characteristics make them

excellent for quick reactions [8], extremely exothermic reactions [9], and explosive reactions [10,11]. Microreactors have grown significantly from their beginnings in analytical applications to the manufacturing of chemicals and even the research of reaction kinetics, gaining the interest of academia and industry [6,12].

The jetting phenomenon in micro-flow systems clearly indicates the important effect of the physical properties of the transported phases on the entire droplet formation system. The creation of droplets is a direct result of fluid instabilities. In a micro-flow system, two possibilities can occur when two immiscible fluids come into direct touch. The first scenario includes droplet production, whereas the second involves jet formation. The flow conditions of the phases and the interfacial tension between the two interacting phases totally determine the production of droplets or jets. Several forces are working on the two phases that form the droplets simultaneously: viscous forces that restrict the expansion of jet deformations vs. inertial forces that favor the production of a long fluid thread. The balance of these forces determines whether droplets or jets develop under specific conditions.

Controlling the droplet's sizes, distribution, and shape is essential in controlling the mass transfer area in any microreactor. Furthermore, the interaction between the reaction phases is important to determine many of the reaction controlling factors that influence the final product properties poorly controlled in bench-scale or industrial-scale systems. Microfluidics technology provided a unique opportunity to tackle the drawbacks of bench-scale reaction systems by providing a controlled droplet generation where each droplet is considered an independent reactor. In the present work, surfactant and polymeric additives were used in minute quantities to investigate their effect on the flow behavior and droplet generation rates in a microfluidics reactor designed and fabricated for this work. The purpose is to compare the droplet-generated size, shape, and distance between the droplets. Other than that, the jetting phenomenon that happens during droplet generation was also investigated. The solution of the polymer (XG) and surfactant (CTAB) was prepared in 5 different concentrations (50, 100, 150, 200, and 250) ppm and (500, 1000, 1500, 2000, and 2500) ppm, respectively. The flow of the continuous and dispersed phases was controlled by varying the pressure ratio of both phases for the droplet to form. The microfluidic chip was connected to an open-loop fluid circulation system, and the produced polymer and surfactant droplet sizes were recorded using a high-resolution microscope and observed.

2. Experimental

2.1 Experimental

In the present work, an anionic polymer XG (xanthan gum) and cationic surfactant CTAB (cetyltrimethylammonium bromide) were used as main additives (dispersed phase), and octanoic acid was used as an oil (continuous phase). The materials were purchased from Sigma-Aldrich and used without any further treatment. Xanthan gum (XG) and Cetyltrimethylammonium bromide (CTAB) were dissolved in deionized (DI) water using a magnetic stirrer to prepare solutions with five different concentrations (50, 100, 150, 200, 250 ppm) and (500, 1000, 1500, 2000 and 2500 ppm) respectively. The concentration ranges for the polymeric additive and the surfactant additive were chosen to prevent massive changes in the transported phases' apparent physical properties that might result in a demulsification instead of an emulsification action known at very high addition concentrations. The viscosity of the octanoic acid was 7.7 mPas in the present work. The concentration of the additive addition was calculated based on a weight/weight basis. For example, 0.01 g of XG was added to 100 mL (100 g) of DI water to prepare a 100 ppm solution. The solutions were homogenized for 3 hours via magnetic stirring before the experimental procedure.

2.2 Fabrication Of Microchannels

The photolithography microfabrication method was adopted to fabricate the desired microfluidics chip. Figure 1 summarizes the microfabrication steps of the microchip, and Figure 2 shows the fabricated microchannel. First, a clean 4-inch wafer was coated with 5.6 ml of SU-8 photoresist with a programmable spin coater (model: Laurell, USA) to obtain a thickness of 100 μm . The coated wafer was left to relax on a flat surface for at least 1 hour. Next, the wafer was pre-baked on a hot plate at 65°C for 15 minutes and 95°C for 2 hours. The microchip design was then printed on the wafer using a micron-pattern generator (Heidelberg μPG 101). After the exposure process, the wafer was post-baked on a hot plate at 65°C for 15 minutes and followed by 95°C for 40 minutes. Next, the unexposed SU-8 photoresist was removed by soaking the wafer in 20 ml of SU-8 developer and slightly agitated for 5 minutes. Afterward, the wafer was cleaned with isopropanol followed by ultra-pure water before hard baking at 135°C for 2 hours. Then, PDMS was used as the substrate for the microchannel. The silicone elastomer base (Slygard 184A) and silicone elastomer curing agent (Slygard 184B) with a ratio of 10:1 was mixed using a centrifugal mixer (model: Thinky, Japan). The mixture was then poured on the wafer that was placed in a plastic petri dish. The petri dish was placed in a desiccator (model: Kartell, Italy) for at least 1 hour to remove all the trapped air bubbles. The process is followed by baking the PDMS in an oven for 2 hours, where the PDMS would be solidified. When the PDMS was cooled, the mold was cut using a scalpel and carefully peeled using a tweezer. Next, the inlets and outlet tanks of the microchannel were punched using a puncher. The PDMS and a piece of clean glass were treated in a plasma cleaner (model: Harrick Plasma, USA) for 2 minutes under vacuum conditions. Both surfaces were then brought together and pressed slightly for bonding.

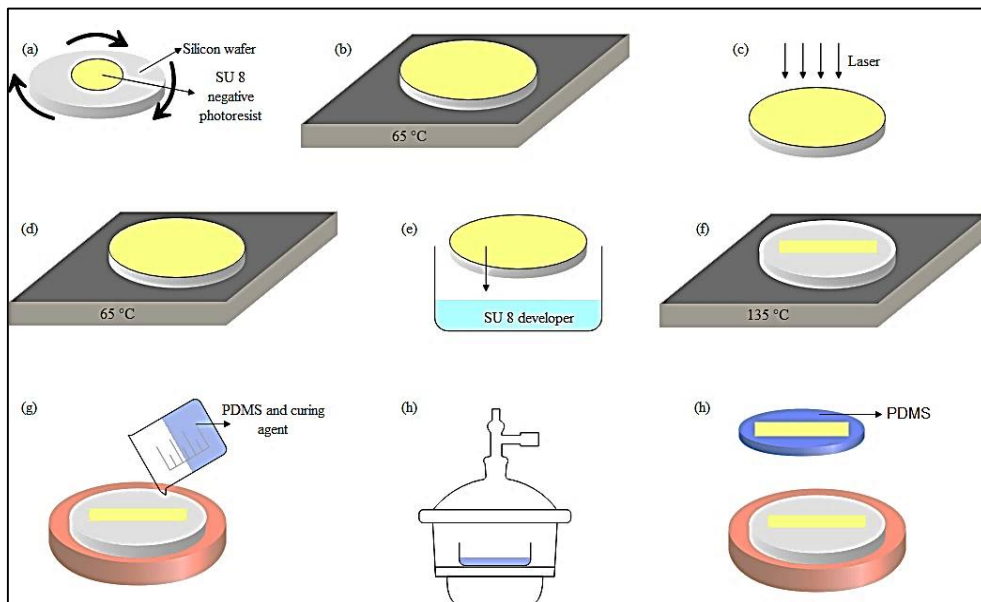


Figure 1: Photolithography Microfabrication method

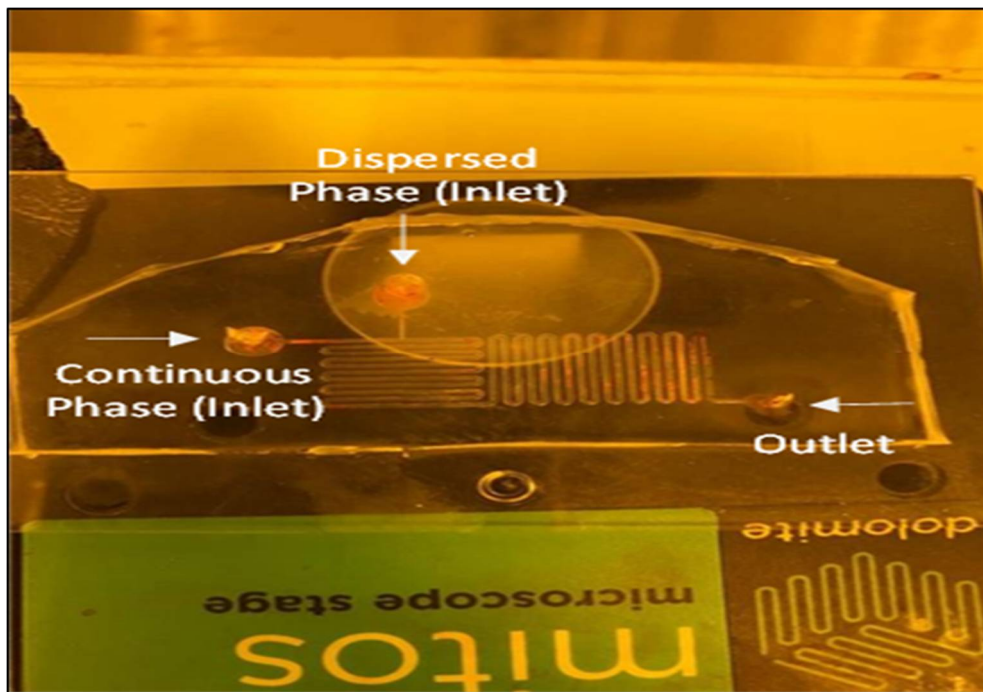


Figure 2: Designated T-junction Microchip

2.3 Microfluidic Flow Setup

Figure 3 below shows the experimental setup used in this work is the same as discussed previously by Abdulbari et al. [1,2,9]. The setup contained a syringe pump (model: SN-50F6), a differential pressure transmitter (model: STK336) with a 0.001 mbar precision, a custom-made thermoplastic polymer (Topas) straight microchannel of $100\ \mu\text{m} \times 100\ \mu\text{m} \times 12\ \text{cm}$ (W x H x L) provided by the Chip-shop in Germany, tube connections, and a beaker, which was the storage container. The setup was completed by connecting the pump with two syringes to the first T-junction using the tube connections. The inlet of the microchannel was connected to the second T-junction, and the outlet was connected to another T-junction. The pressure transmitter was connected in between to measure pressure gradients. Finally, the remaining solution flowed out from the third T-junction and was discharged into the beaker.



Figure 3: Microfluidic experimental setup

2.4 Experimental Procedure

The syringe pump has been filled with the octanoic acid as a continuous phase XG and CTAB as a dispersed phase. Then, the syringe tube was connected to the inlet of the microchip, while another tube was connected from the outlet of the microchip and to the cup as a collecting reservoir. Next, the light of the high-resolution microscope was adjusted according to the examiner's vision. After that, the pressure was applied to both syringes through the computer connected to the Elveflow vacuum and pressure controller and the Elveflow flow sensor. The pressure applied varies to investigate the droplet generated, and the results were recorded and observed using Image J.

3. Result and Discussion

3.1 Effect of Concentration

The sizes of droplets can be affected by flow rates, fluid properties, surface hydrophobicity, and channel dimension. In these cases, we investigated droplets generated by manipulating the flow rates, fluid properties, and surface hydrophobicity of the fluid we used. Figure 4 shows the droplet generation from water-oil based in the T-junction microfluidic chip with a pressure ratio of 305:320 mbar. The water started to shear as the droplet was generated in the oil phase, which is octanoic acid. This is due to the sized droplet emulsions at controlled rates presented. As a result, the shear force is smaller, leading to small, uniform, on-demand, and with-feedback droplets.

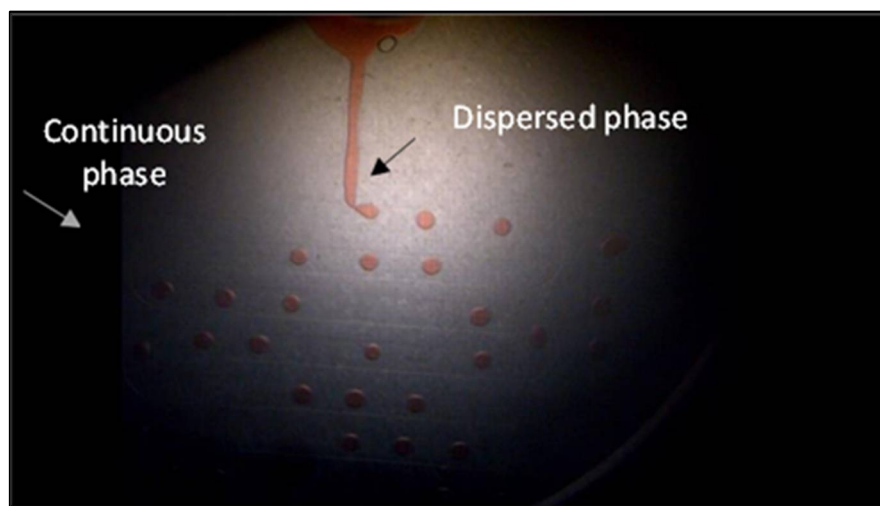


Figure 4: Droplet generation of water-oil in T-junction Microfluidic Chip at a pressure ratio of 305:320 mbar

In this experiment, Xanthan gum polymer and CTAB surfactant were used to modify the apparent physical properties of the dispersed phase. Based on Figure 5 (a), the droplets generated and the diameter of the droplets (Xanthan Gum) at 50 ppm with a pressure ratio of 305:320 mbar were much smaller, and the distance between droplets was larger. This is because xanthan gum provides stability to the emulsion and the lack of dependence on the XG viscosity. The droplet formation process was governed by the properties of the continuous phase (octanoic acid). The non-Newtonian effects exhibit themselves mainly during the droplet breakup stage, where localized shear rates were large. As the concentration increases, the size droplet also increases. This is because of the tendency dispersed phase to generate a droplet with increasing velocity of the continuous phase along with the flow rate, pressure, viscosity of the dispersed phase, and lower interfacial tensions where it can be observed (Figure 5b to e).

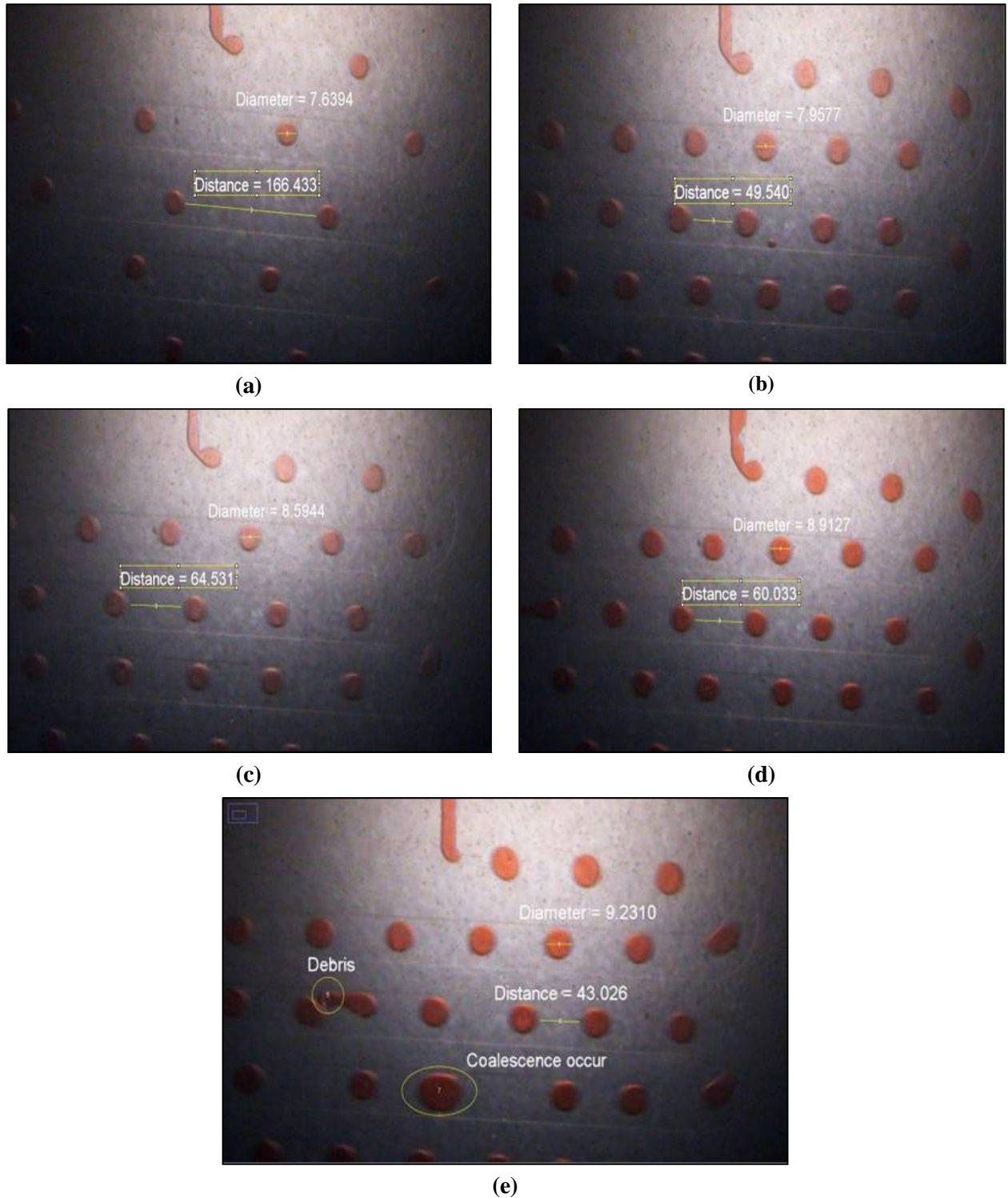


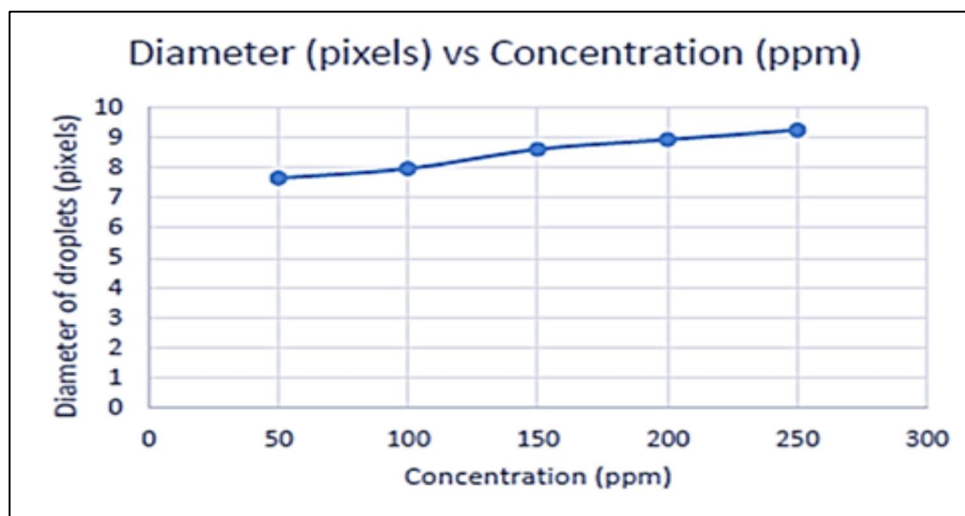
Figure 5: Microscopic image of droplets generation of XG in microflow system at same pressure ratio 305:320 mbar (a) 50 ppm (b) 100 ppm (c) 150 ppm (d) 200 ppm (e) 250 ppm

Other than that, at the highest concentration (250 ppm), in the middle of the flow, coalescence started to happen. This is because the XG concentration is insufficient to spread in an aqueous medium, causing a higher possibility of coalescence after several turns. Besides, as the concentration increases, the interfacial tension also increases, affecting the shorter distance between droplets, and the tendency for the droplet to coalesce was higher.

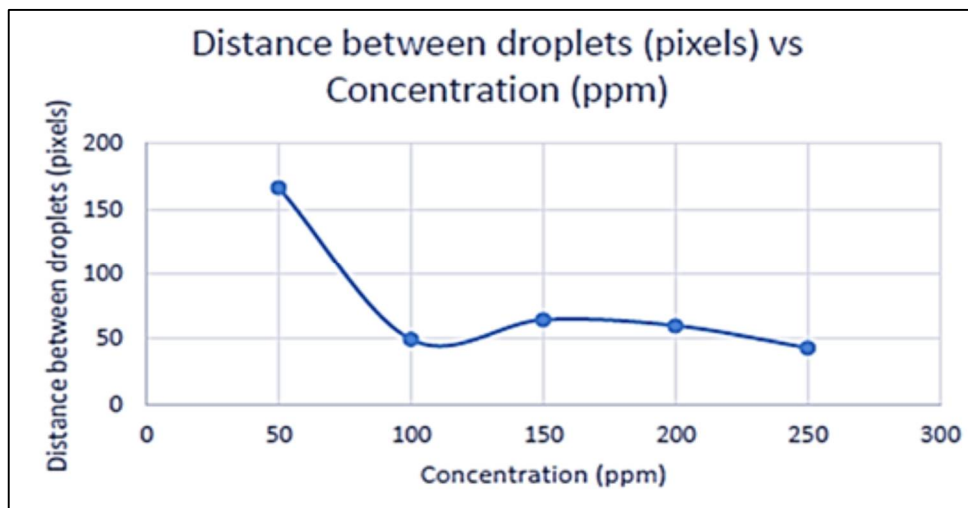
Table 1 and Figure 6 show the relationship between diameter and distance between droplets produced with different concentrations of XG. The droplet diameter increases rapidly as the concentration increases. However, the distance between droplets started to decrease from 50 ppm to 100 ppm, suddenly increasing to 150 ppm before decreasing back to 200 ppm and 250 ppm. It showed that increasing the XG concentration after a certain limit increases the droplet's size, affecting the distance between droplets. Even at higher concentrations, the distance between droplets is not always linear at some point.

Table 1: Summary of diameter and distance between droplets at different concentrations of XG

Concentration (ppm)	Diameter of droplets (pixels)	Distance between droplets (pixels)
50	7.6394	166.433
100	7.9577	49.540
150	8.5944	64.531
200	8.9127	60.033
250	9.2310	43.026



(a)



(b)

Figure 6: (a) Relationship between concentration and diameter of droplets, and (b) the relationship between the concentration and distance between droplets generated by XG

Furthermore, Surfactants, known as Surface Active Agents, are usually used to create emulsions or demulsify pre-created emulsions due to their unique charge character. The presence of surfactant on the two immiscible liquids' interface will change the interface's physical properties depending on the type of surfactant, whether it is a demulsifying or emulsifying agent. Using an emulsifying agent will increase the interfacial tension between two immiscible liquids forming the emulsion, increasing the repulsion forces between the generated droplets and the droplet's sphericity. In this present work, CTAB was used as a dispersed phase since CTAB are cationic surfactants and act as emulsifying agents. It is believed that at the lower surfactant concentration,

the formation of the droplet size is dominant because of the viscosity of the phases, which leads to a smaller droplet. It is also believed that the smaller the droplet, the lesser the number of droplets generated and the further distance between droplets. However, the results show different behavior. As shown in Figure 7a, at 500 ppm of CTAB concentration, droplets formed immediately and rapidly spread the compound in the dispersed phase. The same goes for Figure 7b, except for the droplets being smaller than the previous one. Figure 7c and Figure 7d show that at high concentration, which was 1500 ppm and 2000 ppm, respectively, the size of droplets was smaller, and the droplets generated were also lesser. The distance between droplets became much further. This is due to the higher viscosity of the dispersed phase (CTAB) that limited the shearing force of droplet generation to occur. Besides, increasing the surfactant concentration is believed to reduce the interfacial tension between two phases, which leads to a decrease in droplet size. The reduction in droplet size was usually affected by an increase in surface area. Thus, the aggregation of the uncovered surface competes with the primary coverage process of newer surfaces. So, increasing the surfactant causes the newly generated droplet's surfaces to be covered quickly, resulting in smaller droplets produced.

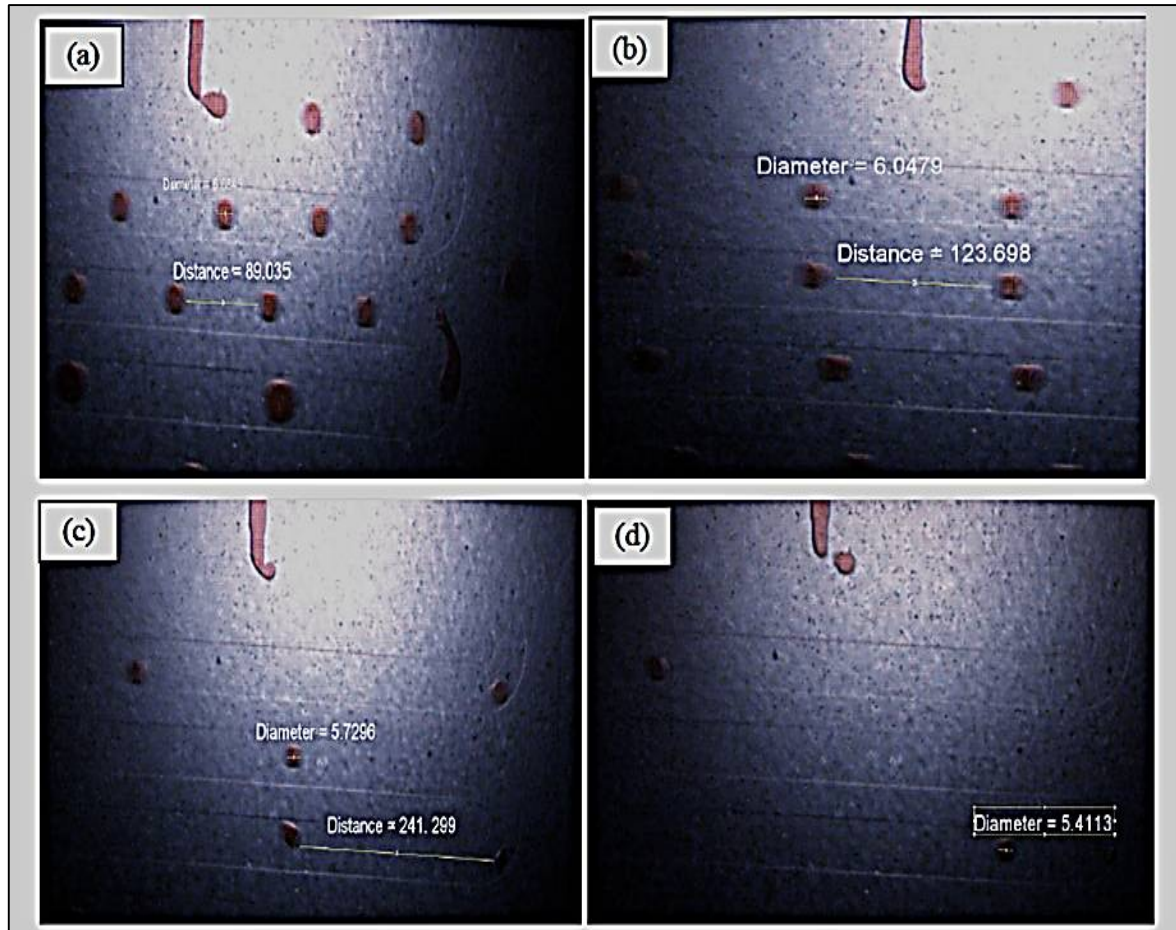
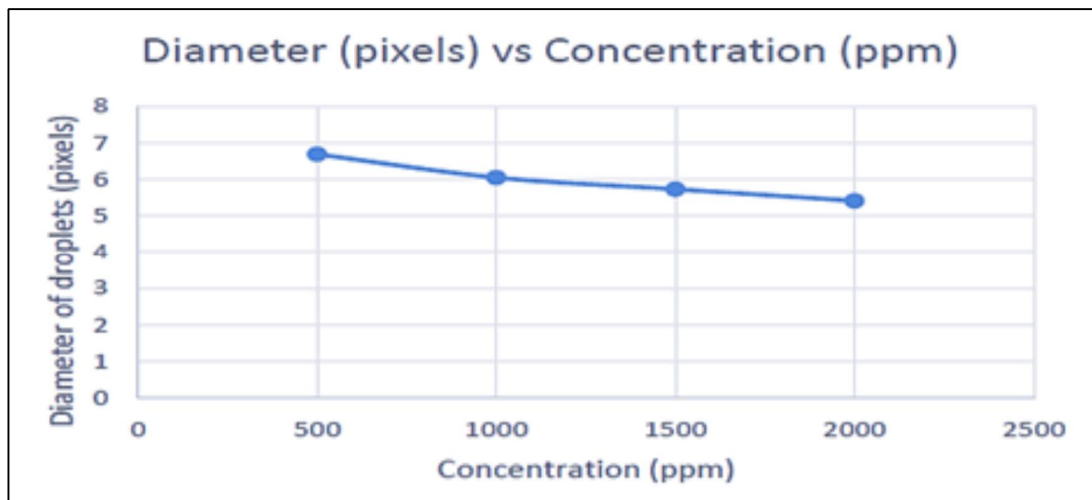
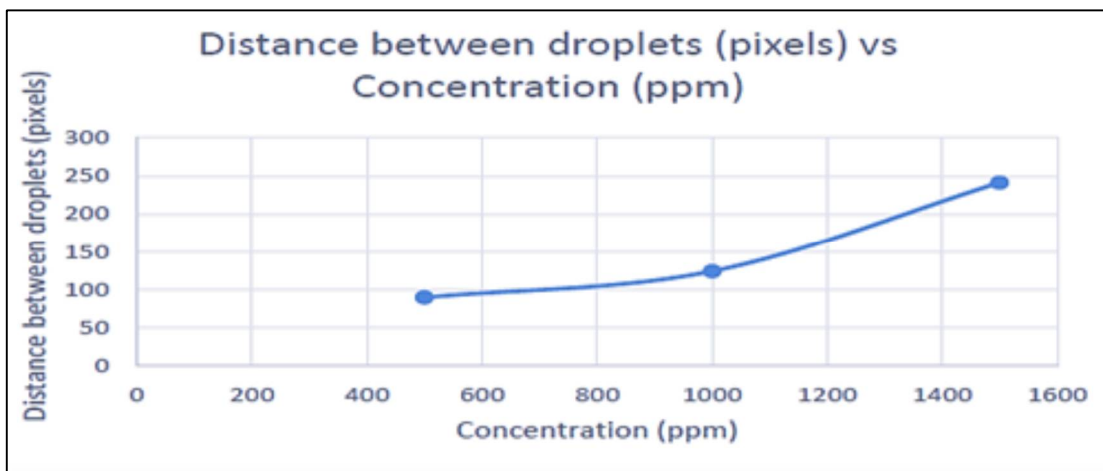


Figure 7: Microscopic image of droplets generation of XG in microflow system at same pressure ratio 305:320 mbar (a) 500 ppm (b) 1000 ppm (c) 1500 ppm (d) 2000 ppm

Figure 8 and Table 2 show the relationship between CTAB concentration and diameter of droplets and the distance between droplets generated. As the surfactant concentration increases, the droplet size produced decreases, whereby the diameter of the droplets also decreases while the distance between droplets becomes further. The droplet generation rate becomes lesser due to the viscosity of CTAB being larger than octanoic acid. As the viscosity of CTAB is higher, the pressure applied to the dispersed phase (305 mbar) cannot flow to the main channel to shear and form the droplets. This happens when the dispersed phase resists the deformation of shear stress due to its intermolecular friction, known as shear-thickening. As the viscosity of the dispersed phase increases, the shear rate decreases and leads to the shearing force of the dispersed phase being lesser to form the droplets. Since droplets failed to be formed at lower pressure, the higher pressure needed to apply to the dispersed phase for the fluid to flow to the main channel and sheared off easily to produce the droplets.



(a)



(b)

Figure 8: (a) Relationship between concentration and diameter of droplets, and (b) the relationship between the concentrations and the distance between droplets generated by CTAB

Table 2: Summary of diameter and distance between droplets at different concentrations of CTAB

Concentration (ppm)	Diameter of droplets (pixels)	Distance between droplets (pixels)
500	6.6845	89.035
1000	6.0479	123.698
1500	5.7298	241.299
2000	5.4113	>300

3.2 Effect of Jetting Regimes

Figure 9 illustrates jetting regime that occurs while running the experiment. When the pressure of both the continuous and dispersed phases increases, droplets are formed in jetting mode. The dispersed phase enters the main channel as a liquid jet that is eventually broken up into droplets due to the instability of the interface. Based on Figure 9a, Figure 9d, and Figure 9e, the dispersed phase undergoes jetting mode before it forms into the droplet. Droplets formed in the mode can either flow through the channel as a spherical droplet or a liquid plug, depending on the relative flow rates and pressure of the continuous and dispersed phases. The jet length follows a linear relationship with the flow rate and pressure at given viscosity and viscosity ratio. Therefore, different droplet formation patterns can occur as a function of the viscosity ratio.

However, Figures 9b and 9c show the opposite results. The jetting regime occurs without generating the droplets at all when the dispersed phase flows into the main channel. At higher pressure that has been applied, the shear force failed to occur and led to the failure of droplet generation. This is because XG shows no viscoelastic enhancement, but their dynamics are strongly slowed. As a result, jet breakup length increased with jet flow rate for all measured flow rates. In this case, at a higher pressure ratio of 150 ppm and 200 ppm of XG, the jet breakup length does not break into droplets, except it keeps continuously lengthening until the end. Further increase of pressure causes a deformation of jet breakup length and droplets not generated.

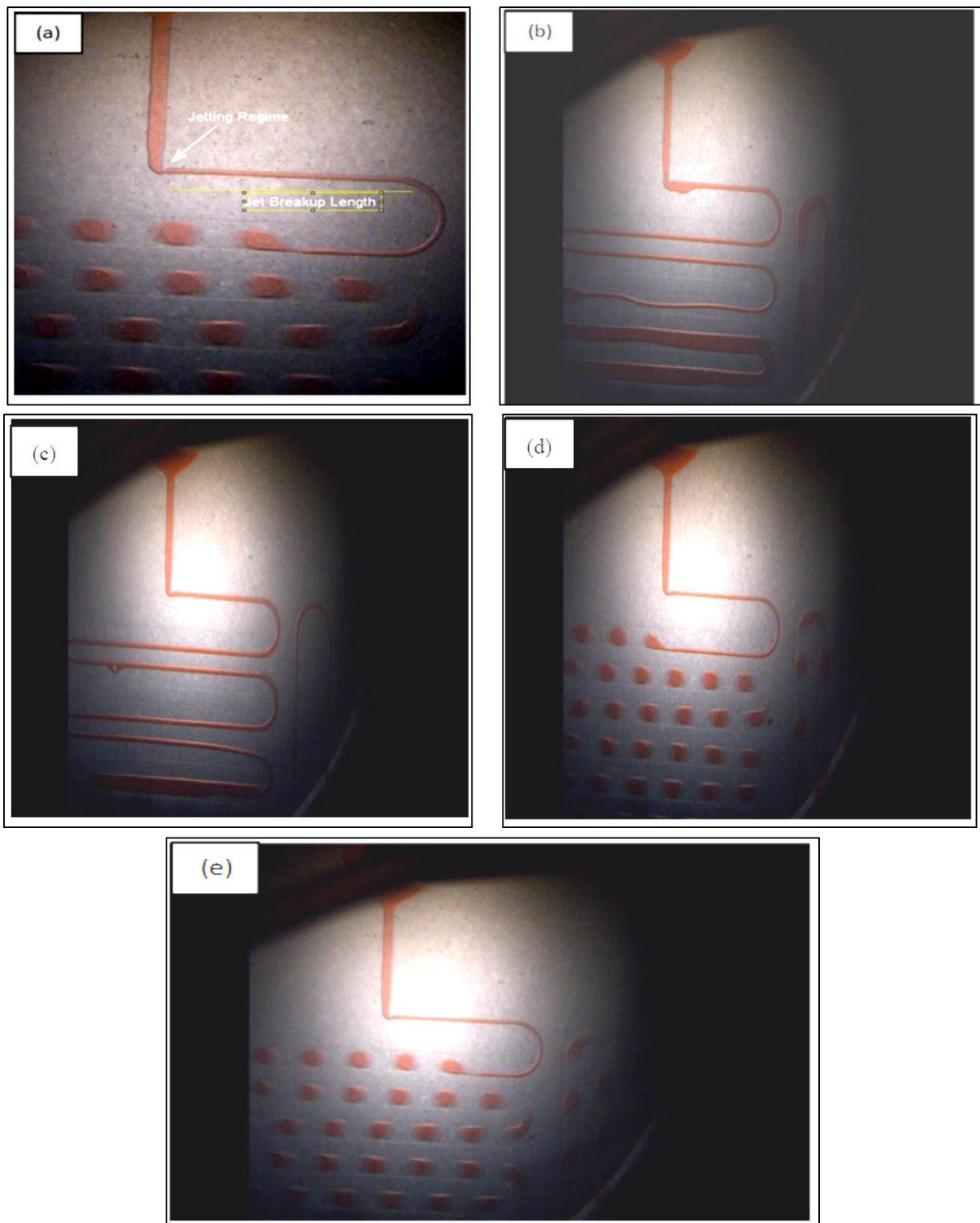


Figure 9: Microscopic images of Jetting Regime at a higher pressure of dispersed phase on different concentrations (a) 610 mbar of 100 ppm of XG (b) 620 mbar of 150 ppm of XG (c) 615 mbar of 200 ppm of XG (d) 620 mbar of 500 ppm of CTAB (e) 695 mbar of 1500 ppm of CTAB

4. Conclusion

This work aims to introduce a new polymer-surfactant complex behavior in a microfluidic system and to investigate droplets size, shape, and distance between droplets generated by polymer (XG) and surfactant (CTAB) and the effect of the jetting regime on the complexes. Droplet formation of XG and CTAB in microfluidic chip were recorded using a high-resolution microscope and observed using Image J. From the result, droplets generated from XG have a larger size, and the distance between droplets generated is shorter. The diameter size of droplet formation increases as the concentration increases at the constant pressure ratio of the continuous and dispersed phases. As the distance between droplets got shorter, the possibility of the coalescence happening after several turns were higher since the interfacial tension between droplets was stronger. Meanwhile, droplets generated from

CTAB have the opposite result as smaller droplet sizes, and the distance between droplets was further as the concentration increased. Introducing surfactants in the system helps reduce the interaction forces between liquid molecules. Thus, it will reduce the viscosity and leads to more droplet generation. However, CTAB shows the droplet generation becomes lesser as the concentration increases. Furthermore, increasing pressure ratio affects the jetting regime in the micro-flow system. As the pressure ratio increases, the droplet formed flows through the main channel as a liquid plug, whereas it undergoes the jet breakup length before the dispersed phase shearing off and forming the droplet. At some point, the droplet failed to produce the dispersed phase with a jet breakup length deformation, resulting in the dispersed phase flowing as a liquid jet until the end of the flow.

Acknowledgment

The authors wish to acknowledge and appreciate the unlimited support of the Center of Excellence for Advanced Research in Fluid flow and University Malaysia Pahang.

Author contribution

All authors contributed equally to this work.

Funding

This research received no external funding

Data availability statement

The data that support the findings of this study are available on request from the corresponding author.

Conflicts of interest

Authors declare that their present work has no conflict of interest with other published works.

References

- [1] H.A. Abdulbari, E. Basheer, Microfluidic Desalination: A New Era towards Sustainable Water Resources, *ChemBioEng Rev.*, 8 (2021) 121–133. <https://doi.org/10.1002/cben.202000023>
- [2] H.A. Abdulbari, E.A. Basheer, Investigating the enhancement of microfluidics-based electrochemical biosensor response with different microchannel dimensions, *Curr. Anal. Chem.*, 13 (2017) 361–369. <https://doi.org/10.2174/1573411012666160920145311>
- [3] L. Capretto, D. Carugo, S. Mazzitelli, C. Nastruzzi, X. Zhang, Microfluidic and lab-on-a-chip preparation routes for organic nanoparticles and vesicular systems for nanomedicine applications, *Adv. Drug Delivery Rev.*, 65 (2013) 1496–1532. <https://doi.org/10.1016/j.addr.2013.08.002>
- [4] D.T. Chiu, A.J. DeMello, D. di Carlo, P.S. Doyle, C. Hansen, R.M. Maceiczky, R.C.R. Wootton, Small but perfectly formed? Successes, challenges, and opportunities for microfluidics in the chemical and biological sciences, *Chem*, 2 (2017) 201–223. <https://doi.org/10.1016/j.chempr.2017.01.009>
- [5] F. Fanelli, G. Parisi, L. Degennaro, R. Luisi, Contribution of microreactor technology and flow chemistry to the development of green and sustainable synthesis, *Beilstein J. Org. Chem.*, 13 (2017) 520–542. <https://doi.org/10.3762/bjoc.13.51>
- [6] Z.V. Feng, K.R. Edelman, B.P. Swanson, Student-fabricated microfluidic devices as flow reactors for organic and inorganic synthesis, *J. Chem. Educ.*, 92 (2015) 723–727. <https://doi.org/10.1021/ed5005307>
- [7] D.E. Fitzpatrick, C. Battilocchio, S. v Ley, Enabling technologies for the future of chemical synthesis, *ACS Cent. Sci.*, 2 (2016) 131–138. <https://doi.org/10.1021/acscentsci.6b00015>
- [8] E.D. Lavric, C. Cerato-noyerie, Mass transfer in gas-liquid flow in Corning® Advanced-Flow™ Reactors, *Chem. Eng. Trans.*, 29 (2012) 979–984. <https://doi.org/10.3303/CET1229164>
- [9] F.W.M. Ling, W.K. Mahmood, H.A. Abdulbari, Rapid Prototyping of Microfluidics Devices using Xurography Method, in: *MATEC Web of Conferences, Fluids and Chemical Engineering Conference*, 111, 2017,5. <https://doi.org/10.1051/mateconf/201711101009>
- [10] J. Pelleter, F. Renaud, Facile, fast and safe process development of nitration and bromination reactions using continuous flow reactors, *Org. Process Res. Dev.*, 13 (2009) 698–705. <https://doi.org/10.1021/op8002695>
- [11] T.W. Phillips, I.G. Lignos, R.M. Maceiczky, A.J. DeMello, J.C. DeMello, Nanocrystal synthesis in microfluidic reactors: Where next?, *Lab on a Chip*, 14 (2014) 3172–3180. <https://doi.org/10.1039/C4LC00429A>
- [12] R. Porta, M. Benaglia, A. Puglisi, Flow chemistry: Recent developments in the synthesis of pharmaceutical products, *Org. Process Res. Dev.*, 20 (2016) 2–25. <https://doi.org/10.1021/acs.oprd.5b00325>